The following article appeared in Water Science and Engineering Volume 16, Issue 2, June 2023, Pages 143-153 and may be found at: https://doi.org/10.1016/j.wse.2022.12.004

Water Science and Engineering 2023, 16(2): 143−153

HOSTED BY

ELSEVIER

Available online at www.sciencedirect.com

Water Science and Engineering

journal homepage: wse.hhu.edu.cn

Simultaneous nitrification and autotrophic denitrification in fluidized bed reactors using pyrite and elemental sulfur as electron donors

Maria F. Carboni [a,*], Sonia Arriaga [a,b], Piet N.L. Lens [a]

[a] National University of Ireland Galway, H91 TK33 Galway, Ireland
[b] Instituto Potosino de Investigación Científica y Tecnológica, 78216 San Luis Potosí, Mexico

Received 27 June 2022; accepted 14 November 2022
Available online 26 December 2022

Abstract

In this study, simultaneous nitrification and autotrophic denitrification (SNAD) with either elemental sulfur or pyrite were investigated in fluidized bed reactors in mesophilic conditions. The reactor performance was evaluated at different ammonium (12−40 mg/L of NH_4^+-N), nitrate (35−45 mg/L of NO_3^--N), and dissolved oxygen (DO) (0.1−1.5 mg/L) concentrations, with a hydraulic retention time of 12 h. The pyrite reactor supported the SNAD process with a maximum nitrogen removal efficiency of 139.5 mg/(L·d) when the DO concentration was in the range of 0.8−1.5 mg/L. This range, however, limited the denitrification efficiency of the reactor, which decreased from 90.0% ± 5.3% in phases II−V to 67.9% ± 7.2% in phases VI and VII. Sulfate precipitated as iron sulfate ($FeSO_4/Fe_2(SO_4)_3$) and sodium sulfate (Na_2SO_4) minerals during the experiment. The sulfur reactor did not respond well to nitrification with a low and unstable ammonium removal efficiency, while denitrification occurred with a nitrate removal efficiency of 97.8%. In the pyrite system, the nitrifying bacterium *Nitrosomonas* sp. was present, and its relative abundance increased from 0.1% to 1.1%, while the autotrophic denitrifying genera *Terrimonas*, *Ferruginibacter*, and *Denitratimonas* dominated the community. *Thiobacillus*, *Sulfurovum*, and *Trichlorobacter* were the most abundant genera in the sulfur reactor during the entire experiment.

Keywords: Pyrite; Elemental sulfur; Simultaneous nitrification and denitrification; Nitrogen removal; 16S rRNA

1. Introduction

Secondary effluents coming from anaerobic digestors are commonly characterized by low organic carbon content, but contain high nitrogen concentrations in the form of ammonium (500−1 500 mg/L of NH_4^+-N) to be directly discharged in water bodies (Chen et al., 2015; Park et al., 2010). Conventional processes of treating these effluents generally make use of two different reactors for sequential autotrophic nitrification and heterotrophic denitrification (Drewnowski et al., 2021). This requires the addition of an exogenous carbon source (Guerrero and Zaiat, 2018). However, the need of a more cost-effective configuration of wastewater treatment plants brings new challenges, such as waste sludge reduction, low carbon footprint, and the reduction of used reactor volumes (Hakanen et al., 2011). For these reasons, the conversion to a completely autotrophic process without the addition of a carbon source and the simultaneous nitrification−autotrophic denitrification (SNAD) process are good alternatives to conventional treatments. Autotrophic microorganisms have a lower cell yield that results in less sludge production (Kostrytsia et al., 2018), and this together with no requirement of organic carbon results in lower costs and no CO_2 production during the denitrification process. Moreover, contemporary decontamination from ammonium and nitrate in the same environment reduces the reactor volume required for the treatment.

This work was supported by the Science Foundation Ireland (SFI) through the SFI Research Professorship Programme entitled "Innovative Energy Technologies for Biofuels, Bioenergy and a Sustainable Irish Bioeconomy" (IETSBIO^3; Grant No. 15/RP/2763) and the Research Infrastructure Research Grant Platform for Biofuel Analysis (Grant No. 16/RI/3401).

* Corresponding author.
E-mail address: m.carboni2@nuigalway.ie (Maria F. Carboni).

Peer review under responsibility of Hohai University.

https://doi.org/10.1016/j.wse.2022.12.004

Common inorganic compounds used as electron donors for autotrophic denitrification are reduced sulfur compounds (RSC), such as sulfide (S^{2-}), elemental sulfur (S^0), and thiosulfate ($S_2O_3^{2-}$) (Chung et al., 2014; Dolejs et al., 2015; Shao et al., 2010). Several bacteria, such as *Thiobacillus*, *Pseudomonas*, *Sulfurimonas*, and *Thioprofundum* sp., are able to exploit RSCs as electron donors, exploit nitrate as a final electron acceptor, and convert nitrate to dinitrogen gas (Carboni et al., 2021; Pu et al., 2015; Jørgensen et al., 2009). Pyrite (FeS_2) has been an alternative electron donor for autotrophic denitrification systems in the last two decades. Pyrite is an abundant sulfur-iron mineral present in the earth's crust (Di Capua et al., 2019) and can play a role as an electron donor for nitrate reduction in natural ecosystems (Jørgensen et al., 2009). Several studies have been conducted to investigate pyritic minerals during autotrophic denitrification and to understand the mechanisms of the process. Compared to RSCs, FeS_2 as an electron donor has several advantages when sulfur compounds are applied, such as low sulfate production, no need for external buffer addition, and no production of odorous emissions. Moreover, it is an extremely cheap substrate because it is usually recovered as a waste material from the mining sector (Ferreira et al., 2021).

Not many investigations have been done on SNAD processes (Guerrero and Zaiat, 2018; Hwang et al., 2005), and pyrite as an electron donor was only reported by Li et al. (2020) and Li et al. (2021). In this study, two fluidized bed reactors (FBRs) were used to simultaneously remove ammonium and nitrate with either elemental sulfur or pyrite as an electron donor for the denitrification process. The stoichiometric reaction involved in aerobic nitrification and anoxic denitrification have been reported as follows (Bosch et al., 2012; Cardoso et al., 2006; Hoffmann et al., 2007):

$$NH_4^+ + 2O_2 \rightarrow NO_3^- + 2H^+ + H_2O \quad (1)$$

$$FeS_2 + 3NO_3^- + 2H_2O \rightarrow Fe(OH)_3 + 1.5N_2 + 2SO_4^{2-} + H^+ \quad (2)$$

$$5S^0 + 6NO_3^- + 2H_2O \rightarrow 5SO_4^{2-} + 3N_2 + 4H^+ \quad (3)$$

However, the presence of oxygen in bioreactors can bring several unwanted secondary reactions of pyrite (Eqs. (4) and (5)) and elemental sulfur oxidation (Eq. (6)), which could limit the autotrophic denitrification reaction (Lehner et al., 2007; Mora et al., 2016):

$$4FeS_2 + 14O_2 + 4H_2O \rightarrow 4Fe^{2+} + 8SO_4^{2-} + 8H^+ \quad (4)$$

$$4Fe^{2+} + O_2 + 4H^+ \rightarrow 4Fe^{3+} + 2H_2O \quad (5)$$

$$S^0 + 1.5O_2 + H_2O \rightarrow SO_4^{2-} + H^+ \quad (6)$$

This study aimed to investigate the effect of the dissolved oxygen (DO) concentration on nitrification, S^0-driven autotrophic denitrification and FeS_2-driven autotrophic denitrification. In addition, the nitrogen removal performances of two FBRs were monitored and compared, and the solid by-products generated in the FBRs were identified.

2. Materials and methods

2.1. Inoculum and synthetic wastewater

The microbial community used in this study originated from different sources of inocula. In a pyrite reactor (PR), an enriched denitrifying culture was used, obtained from an FBR operating for 220 d at mesophilic temperature (30°C) for pyrite-driven autotrophic denitrification (detailed in Carboni et al. (2022)). In a sulfur reactor (SR), a specialized autotrophic denitrifying microbial community from an FBR for sulfur-driven autotrophic denitrification (see details in Carboni et al. (2022)) was used. Both reactors were further inoculated with nitrifying sludge from a membrane aerated biofilm reactor of the Oxy-Mem wastewater treatment plant (Athlone, Co. Westmeath, Ireland). In addition to the first inoculation on day 0, 50 mL of nitrifying sludge was added in both reactors on day 49.

Mineral medium was prepared according to Stams et al. (1993) and modified with 0.41 g/L of KH_2PO_4, 0.53 g/L of $Na_2HPO_4{\cdot}2H_2O$, 0.3 g/L of NaCl, 0.1 g/L of $MgCl_2{\cdot}6H_2O$, 0.11 g/L of $CaCl_2{\cdot}2H_2O$, and 4 g/L of $NaHCO_3$. 0.2 mL/L of vitamin stock solution, 1 mL/L of acid trace element solution, and 1 mL/L of alkaline trace element solution were also added. The pH of the medium was kept in the range of 7.0−7.5. Nitrate was added as KNO_3 at NO_3^--N concentrations of 34−45 mg/L depending on operational periods (Table 1). Ammonium was added in the form of NH_4Cl at NH_4^+-N concentrations of 0−39 mg/L depending on operational periods (Table 1).

2.2. Bioreactor set-up

Two identical glass-made FBRs with volumes of 1 020 mL (800 mL of working volume and 220 mL of headspace) were used in this study (Fig. 1). They were inoculated (30% in volume ratio) with the aforementioned microbial community. The reactors were flushed with N_2 for 20 min to ensure anoxic

Table 1
Operational conditions of FBRs in this study.

Phase	HRT (h)	Time (d)	Influent NH_4^+-N concentration (mg/L)	Influent NO_3^--N concentration (mg/L)	DO concentration (mg/L)
I (batch mode)		0−12			
II	12	13−19	0	45	0
III	12	20−42	12	34	0.1−0.3
IV	12	43−60	12	34	0.3−0.9
V	12	61−73	24	34	0.3−0.9
VI	12	74−82	24	34	0.8−1.5
VII	12	83−93	39	34	0.8−1.5

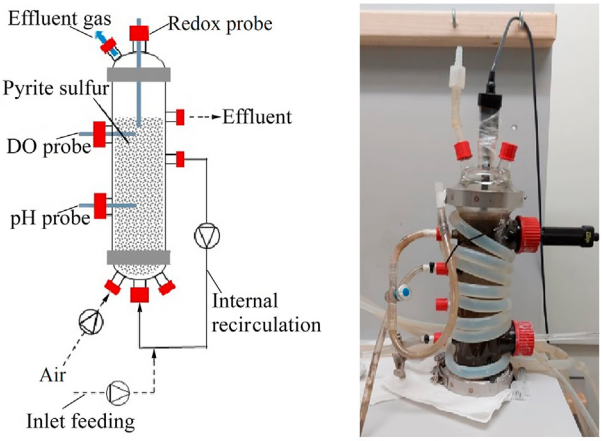

(a) Schematic representation of FBR (b) Photo of FBR

Fig. 1. Schematic representation and photo of FBR used in this study.

conditions. Temperature in the FBRs was maintained at 30°C with a thermostatic recirculation bath. pH was measured in continuous operation with a pH-meter 300 pH/ORP (Cole Parmer, Vernor Hill, USA) and an electron probe with a ceramic junction (VWR, Radnor, USA). DO (Intellical LDO101, Hach, Cork, Ireland) and oxidation-reduction potential (Intellical MTC101, Hach, Cork, Ireland) values were monitored in continuous mode as well.

50 g of FeS_2 (higher than 99% grade and 0.15−0.48 cm in diameter; Fischer Scientific, Hampton, USA) and 30 g of chemically synthetized S^0 (higher than 98% grade and 150 μm in diameter; Fischer Scientific, Hampton, USA) were added to the FBRs as electron donors with a static bed depth of approximately 5 cm. Moreover, in the SR, 30 g of $CaCO_3$ (higher than 98% grade; Fischer Scientific, Hampton, USA) was also used as buffer material. Liquid inside the column was continuously recirculated in upflow mode with a peristaltic pump (Masterflex Cole Parmer, Chicago, USA) at a flow rate of 200 mL/min that allowed a bed expansion of 35%−40% in both reactors. A peristaltic pump (Masterflex Cole Palmer, Chicago, USA) was also used to feed the synthetic wastewater to the FBRs and pump out the effluent. Air was introduced to provide oxygen for nitrification through a porous stone installed at the bottom of the FBRs to ensure smooth mass transfer with a peristaltic pump (Verderflex EV045 Economy, Castleford, United Kingdom).

2.3. Start-up and operation of FBRs

The start-up of the FBRs was done in batch mode throughout phase I. During the first 12 d, five batch denitrification cycles were performed to allow the acclimation of microorganisms and their attachment on sulfur or pyrite particles. In this phase, no NH_4^+ or DO was provided to the reactors to restore the environmental conditions in the previous experiment that consisted of a 220-d experiment of autotrophic denitrification using either pyrite or elemental sulfur in the FBRs (Carboni et al., 2022). From day 13 to day 93 (phases II−VII), the reactors were operated in continuous mode under different operating conditions summarized in Table 1. In the PR and SR, the same synthetic wastewater was introduced as the influent, and pH was always kept in the range of 6.9−7.4. The hydraulic retention time (HRT) was constant at 12 h, and NH_4^+-N, NO_3^--N, or DO concentrations were variating. In phase II, only NO_3^- was introduced as the pollutant in the influent at a NO_3^--N concentration of 45 mg/L. From day 20 onwards (phase III), NH_4^+ was also fed in the influent with an initial NH_4^+-N concentration of 12 mg/L. Together with the ammonium supply, NO_3^--N concentration was decreased to 34 mg/L and kept constant in the remaining reactor run. During phases IV−VII, the influent NH_4^+-N concentration was increased up to 39 mg/L, and DO concentration was increased to 1.5 mg/L. Intermittent aeration and no-aeration times were defined with the aid of the DO sensor, using a timer that was set to keep the ranges reported in Table 1. Liquid samples were daily collected from the FBR effluents, and solid samples were taken at the end of each phase.

2.4. Microbial community analysis

Samples for microbial community analysis (10 mL) were collected on days 0, 19, 61, and 93 from both FBRs. All samples were stored at −80°C after snap-freezing in liquid nitrogen. The QIAGEN DNeasy power soil kit (QIAGEN, Hilden, Germany) was used for DNA extraction according to the manufacturer's protocol. The concentration of the extracted DNA was quantified with a Qubit fluorometer (Invitrogen, Carlsbad, CA, USA). Extracted DNA samples were kept at −20°C prior to sequencing. Polymerase chain reaction (PCR) amplification and purification, library preparation, and sequencing were carried out at the Novogene Institute (Beijing, China) on the Illumina NovaSeq 6000 platform. Specific universal primers (515F−806R) were used to amplify the V4 region. Bioinformatic analyses (e.g., operational taxonomic unit (OTU) analysis and alpha and beta diversity analyses) were conducted at the Novogene Institute, as described in detail by Jiang et al. (2019). The processed Illumina NovaSeq 6000 reads were deposited in the Sequence Read Archive of the National Center of Biotechnology Information under accession number PRJNA872858.

2.5. Analytical method

Liquid samples were filtered on 0.22-μm cellulose acetate filters before chemical analyses. Nitrate, nitrite, and sulfate concentrations were determined with ion chromatography using a Dionex Aquion equipped with an AS14A column of 4 mm × 250 mm, an AG14A guard column of 4 mm × 50 mm, and a suppressed conductivity detector (ThermoFisher Scientific, Waltham, MA, USA). The mobile phase was composed of a mixture of Na_2CO_3 (3.03 mmol/L) and $NaHCO_3$ (0.97 mmol/L) at 1.0 mL/min (Florentino et al., 2020). Ammonium and ferrous iron concentrations were measured using a Gallery + nutrient analyzer (Thermo Scientific) following the manufacturer's protocol. Total organic carbon (TOC) was measured with a TOC analyzer (TOC-L, Shimadzu, Kyoto, Japan).

Solid samples were analyzed with a Fourier transform infrared attenuated total reflectance (FTIR-ATR) spectrophotometer (ATR-Nicolet iS5, Thermo Scientific, Waltham, USA) in the range from 4 000 cm^{-1} to 525 cm^{-1} with a resolution of 4 cm^{-1}.

3. Results

3.1. Performance of reactors

3.1.1. Ammonium removal

3.1.1.1. Nitrification in PR. From day 20 onwards, NH_4^+ was introduced in both FBRs through the influent at NH_4^+-N concentration of 12 mg/L. The PR FBR had an unstable nitrification activity during phase III with NH_4^+-N concentration ranging from 3 mg/L to 14 mg/L. On day 43, DO concentration increased from 0.1−0.3 mg/L to 0.3−0.9 mg/L. After this change and the addition of the nitrifying sludge on day 49, a better nitrification activity was achieved on day 51 with an average ammonium removal efficiency of 65%. During phase V, the nitrification activity decreased in the first seven days after NH_4^+-N concentration was increased to 24 mg/L. After that, it recovered up to 50.8%. The increase in DO concentration during phase VI (0.8−1.5 mg/L) allowed a better nitrification. NH_4^+-N concentration in the effluent was 5.8 mg/L on average with a NH_4^+ removal efficiency up to 94.9% on day 82. During phase VII, NH_4^+-N concentration in the influent was increased to 39 mg/L, and the PR FBR achieved a nitrification activity of 91.2% that corresponded to a NH_4^+-N loading rate of 71.5 mg/(L·d).

3.1.1.2. Nitrification in SR. The SR FBR did not achieve good and steady nitrification performance during the complete duration of the experiment. In phase III, an unstable nitrification activity was recorded with an average NH_4^+-N concentration of 7.8 mg/L in the effluent. During phase IV, no improvement was detected even after nitrifying sludge was added to the SR and DO concentration was increased. In subsequent phases, nitrification was always low as well (Fig. 2(a)).

3.1.2. Nitrate removal

After 12 d of operation in batch mode, the reactors were continuously operated for 80 days (Table 1). From day 13 during phase II, the FBRs received 45 mg/L of NO_3^--N. During this period, PR and SR obtained denitrification efficiencies of 91.0% and 95.8%, respectively, which corresponded to average NO_3^--N concentrations of (4.10 ± 2.70) mg/L and (2.00 ± 1.02) mg/L in the effluent (Fig. 2(b)). During phase III, NO_3^--N concentration in the influent was reduced to 34 mg/L when NH_4^+ was fed to the reactors. From day 20, the actual nitrate concentration that the reactors treated was the sum of the nitrate fed to the influent tank and the nitrate generated by the nitrification process (Fig. 2(b)). From phase III onwards, a different behavior in the two FBRs was detected (Fig. 2(b)). The SR FBR had a denitrification activity of 97.8% ± 3.58% for the complete duration

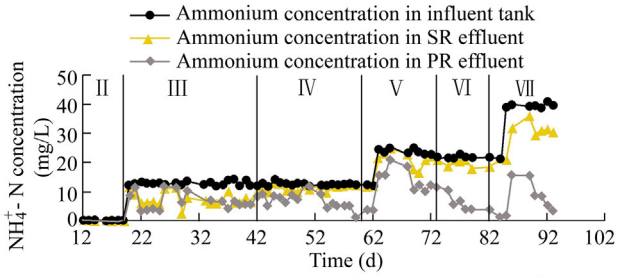

(a) Ammonium concentrations in influent tank, SR effluent, and PR effluent during reactor operation

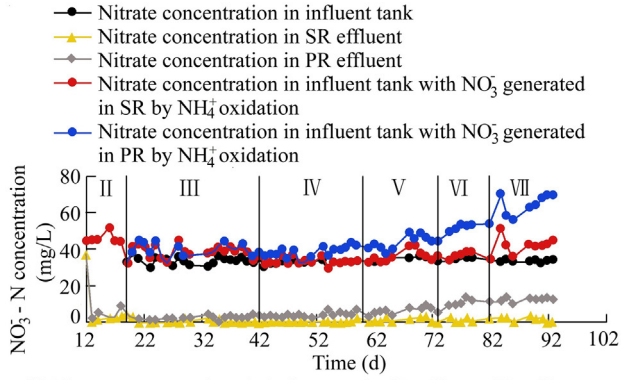

(b) Nitrate concentrations in influent tank, SR effluent, PR effluent, influent tank with NO_3^- generated in SR by NH_4^+ oxidation, and influent tank with NO_3^- generated in PR by NH_4^+ oxidation during reactor operation

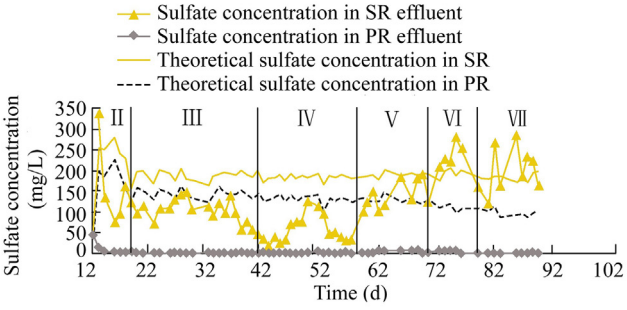

(c) Sulfate concentrations in SR effluent and PR effluent and theoretical sulfate concentrations in SR and PR during reactor operation

Fig. 2. Ammonium, nitrate, and sulfate concentrations during reactor operation.

of the experiment, with a maximum NO_3^--N concentration of 3.20 mg/L in the effluent. The PR FBR, on the other hand, did not show such a stable performance. The nitrate concentration in the effluent increased slowly during the reactor run, with an average NO_3^--N concentration of 11.05 mg/L during phase VII, but the nitrate concentration peaks exceeded the maximum allowable contaminant level (11 mg/L of NO_3^--N) specified in the *World Health Organization Guidelines for Drinking Water Quality*. This decrease in the denitrification activity was concomitant with DO concentration of 0.8−1.5 mg/L in the PR. Moreover, according to ammonium oxidation in phases VI and VII, additional NO_3^--N concentrations up to 20 mg/L on day 82 (phase VI) and 36 mg/L on day 92 (phase VII) were treated by the PR. The actual NO_3^--N loading rate (NLR) that was treated by the PR during phase VII was 139.5 mg/(L·d).

3.1.3. Sulfate production

The production of sulfate during SNAD using sulfurous compounds as electron donors could be due to two different reasons. The denitrification process occurred through the oxidation of S^0 in the SR and S^{2-} in the PR with the concomitant generation of SO_4^{2-}. Alternatively, oxygen required for the nitrification process could also act as an electron acceptor for the oxidation of the present sulfur compounds. In this study, no sulfate was measured in the PR at almost all time points during the reactor run (Fig. 2(c)). On the contrary, SO_4^{2-} was detected in the effluent during each phase in the SR. During phases II−V, its concentration was always below the stoichiometry-based theoretical value that was calculated based on the amount of the reduced nitrate. However, in phases VI and VII, sulfate concentrations were detected to be higher than the theoretical value. In these two phases, DO concentrations in the reactors were in a range of 0.8−1.5 mg/L, which most likely contributed to the sulfur oxidation process.

3.2. Production of solid by-products

Figs. 3 and 4 show the FTIR spectra of the solid samples collected from the bottom of the reactors at the end of each phase. In the PR, three main groups were detected. The first group had wavenumbers of 3 700−2 700 cm^{-1} and exhibited the characteristic peaks of iron sulfate minerals (Majzlan et al., 2011). The second group at 1 600−1 400 cm^{-1} was typical of iron hydroxide ($Fe(OH)_2/Fe(OH)_3$) precipitation (Di Capua et al., 2020). The last group in the wavenumber range of 1 200−800 cm^{-1} was typical of sulfate minerals, such as sodium or calcium precipitates (Kadam et al., 2010; Kiefer et al., 2018). The third group was also present in the SR, confirming that at least part of sulfate was missing in the precipitated solution. Moreover, in the SR, the characteristic peaks of $CaCO_3$ introduced in the reactor as buffer material were detected at wavenumbers of 1 400 cm^{-1}, 900 cm^{-1}, and 700 cm^{-1} (Kiefer et al., 2018).

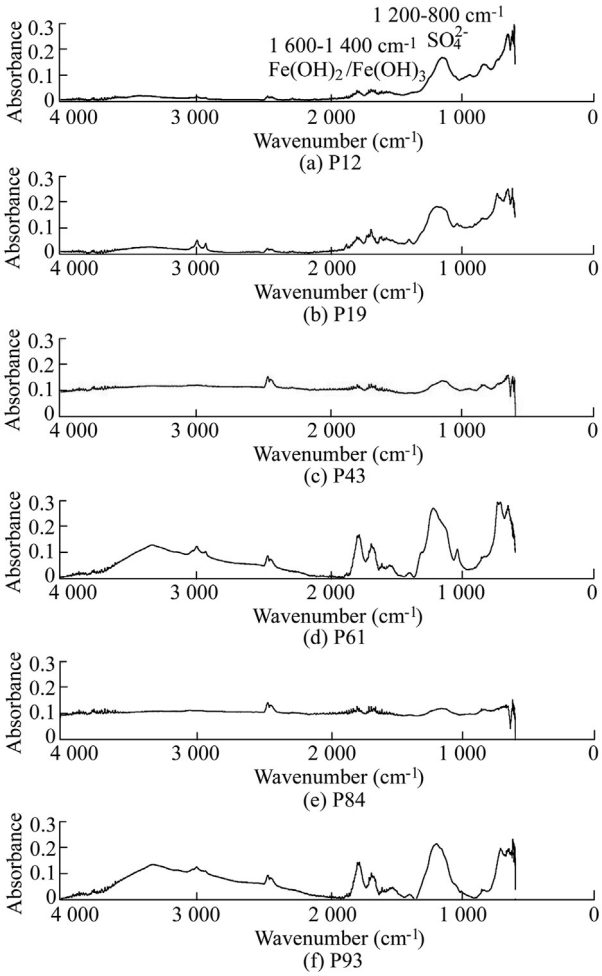

Fig. 3. FTIR spectra of solid deposits collected from PR bottom on operational days 12 (P12), 19 (P19), 43 (P43), 61 (P61), 84 (P84), and 93 (P93).

3.3. Microbial community analyses

3.3.1. Microbial community richness and diversity

The alpha diversity analysis (Table 2) revealed that different microbial communities were present in the elemental sulfur and pyrite FBRs. In the SR FBR, the Shannon index increased from 4.901 to 5.729, and the number of observed species also increased from day 0 to day 93, except for a low decrease on day 19 (Table 2). In the PR FBR, the number of observed species significantly decreased over time, from 1 076 on day 0 to 761 on day 93. In contrast, the Shannon index sharply decreased from day 0 to day 19 but increased to the values above the initial value of day 0 at the last two time points (Table 2).

The principal component analysis (PCoA) of beta diversity (Fig. 5) showed that the microbial communities in the two reactors had a high dissimilarity. In particular, the SR samples were clustered in two groups. One group was related to the first two time points (days 0 and 19), and the other was related to days 61 and 93. The PCoA of the PR showed that the samples at all the four time points were quite diverse, and the sample on day 19 was more distant from the samples at the last two time points than from the sample on day 0 (inoculum). This phenomenon was also shown in the weighted UniFrac distance (Fig. 6(a)). The PR samples collected on day 19 were more similar to the SR samples than to the PR samples collected at other three time points.

3.3.2. Taxonomic diversity

In the SR, the families Comamonadaceae, Hydrogenophilaceae, Sulfurovaceae, Rhodocyclaceae, and Geobacteraceae dominated the microbial community (Fig. 6(b)) for the entire duration, with a total relative abundance (RA) of 70%. At the first two time points, Comamonadaceae and Hydrogenophilaceae had an RA of 50% in total. In contrast, on days 61 and 93, the RA of Hydrogenophilaceae decreased, and RAs of Sulfurovaceae and Geobacteraceae increased. The similarity of the samples at the first two time points agreed with the microbial community richness (Table 2). The most common autotrophic denitrifying genera present in these families were *Thiobacillus* (belonging to Hydrogenophilaceae), *Sulfurovum* (belonging to

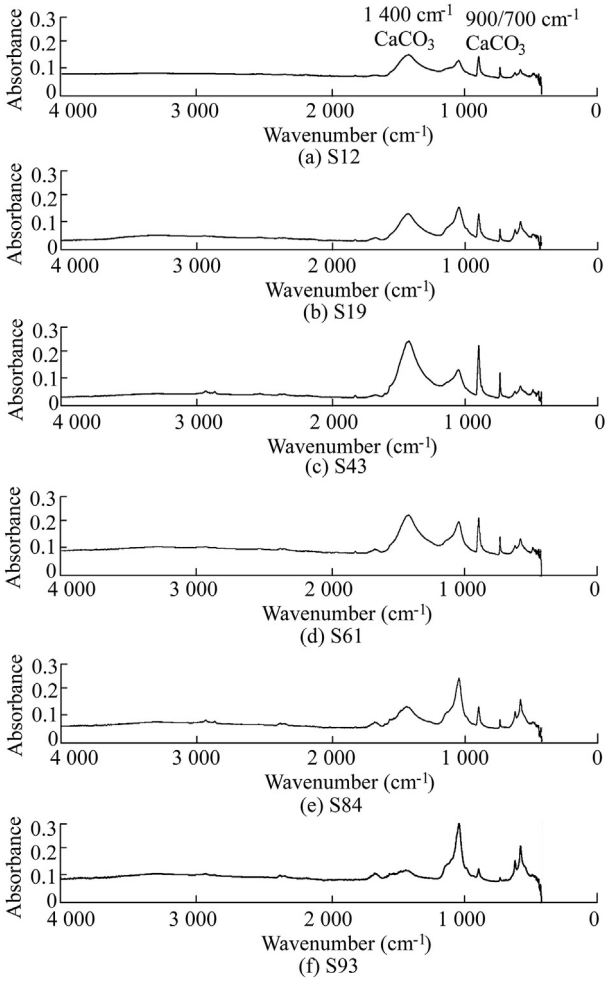

Fig. 4. FTIR spectra of solid deposits collected from SR bottom on operational days 12 (S12), 19(S19), 43 (S43), 61 (S61), 84 (S84), and 93 (S93).

Table 2
Alpha diversity indices and statistical indices of alpha diversity with a clustering threshold of 97% of biomass growing in SR and PR FBRs.

FBR	Sample	Number of observed species	Shannon	Simpson	Chao1	ACE
SR	Inoculum (S0)	782	4.901	0.878	853.823	861.955
	Day 19 (S19)	594	4.741	0.893	627.325	634.241
	Day 61 (S61)	687	5.012	0.899	736.408	735.962
	Day 93 (S93)	1 001	5.729	0.930	1 073.218	1 084.267
PR	Inoculum (P0)	1 076	5.735	0.944	1 156.243	1 173.601
	Day 19 (P19)	863	4.239	0.769	954.766	952.466
	Day 61 (P61)	941	6.289	0.967	1 006.987	1 019.428
	Day 93 (P93)	761	5.970	0.958	813.986	821.094

Note: ACE is the abundance-based coverage estimator.

Sulfurovaceae), *Thiomonas* (belonging to Comamonadaceae), and *Trichlorobacter* (belonging to Geobacteraceae) (Fig. 7). Moreover, other relevant microorganisms common in autotrophic denitrification systems present in the SR (Fig. 7) were *Parvibaculum*, *Ferruginibacter*, *Aerinimons*, *Pseudomonas*, *PHOS-HE36* (belonging to the Ignavibacteriales order), and

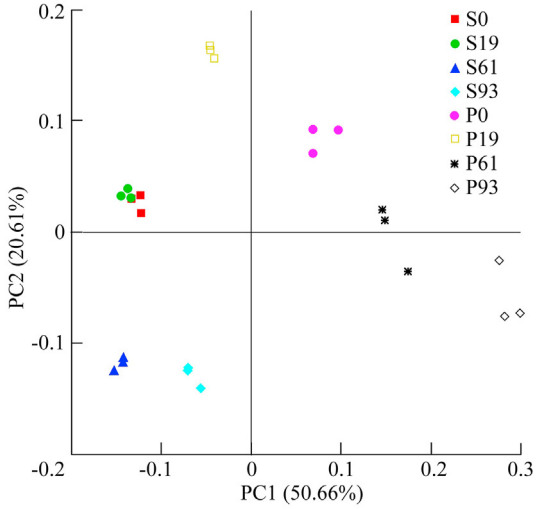

Fig. 5. PCoA of PR and SR samples on operational days 0, 19, 61, and 93.

Ciceribacter (Han et al., 2020; Carboni et al., 2022; Kostrytsia et al., 2018).

The microbial community in the PR on day 0 was composed of Comamonadaceae, Rhodocyclaceae, and Weeksellaceae, with an RA of 70% (Fig. 6(b)). On day 19, almost 70% of the RA was only composed of the Comamonadaceae family, and its RA decreased to 30% at the last two time points. On days 61 and 93, a mixture of other families (Rhodocyclaceae, Chitinophagaceae, and Anaerolineaceae) increased, with an RA of 25%. The most abundant genera in the PR related to SNAD (Fig. 7) on days 0 and 19 were *Cloacibacterium*, *Ferribacterium*, *Dechloromonas*, and *Stenotrophomonas*, and those on days 61 and 93 were *Nitrosomonas*, *Terrimonas*, *Denitratisoma*, and *Anaerolinea*.

4. Discussion

4.1. Simultaneous nitrification and autotrophic denitrification with pyrite as electron donor

This study showed that the removal of NH_4^+ and NO_3^- in one single reactor can be achieved but requires careful selection of the supplied O_2 concentration. The nitrification reaction is an aerobic process, while the denitrification requires anoxic conditions. Autotrophic denitrifying microorganisms are generally facultative anaerobes. Thus, when both oxygen and nitrate are present, the reduction of oxygen preferentially occurs given large free energy (Pochana and Keller, 1999). Another possible side effect of SNAD using pyrite as an electron donor is the release of sulfuric acid, a typical phenomenon of acid mine drainage where FeS_2 is oxidized in the presence of oxygen and at a low pH value (less than 4.5) (Evangelou and Zhang, 1995). For these reasons, the most important parameter of SNAD is the DO concentration in the FBR because low O_2 concentrations could limit nitrification while high O_2 concentrations hamper denitrification and potentially the whole process.

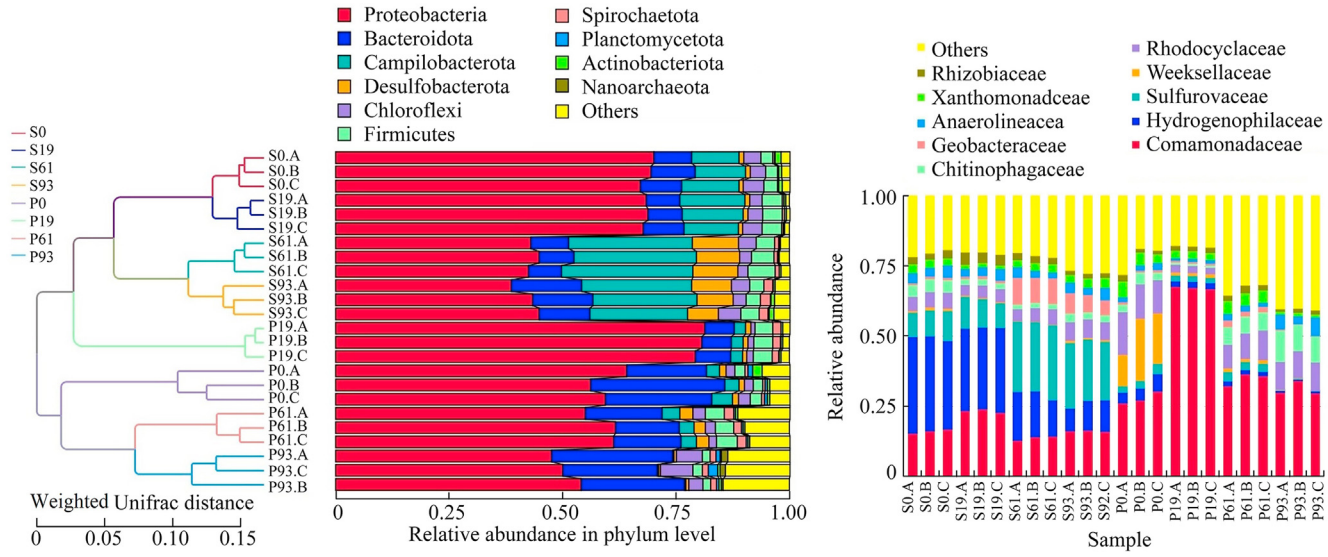

(a) Cluster tree based on weighted Unifrac distances of SR and PR samples on operational days 0, 19, 61, and 93

(b) Bar chart of top ten most abundant families of SR and PR samples

Fig. 6. Cluster tree based on weighted UniFrac distances of SR and PR samples on operational days 0, 19, 61, and 93 and bar chart of top ten most abundant families of SR and PR samples.

This study initially started the experiment with a very low DO concentration in the range of 0.1−0.3 mg/L during phase III. Subsequently, the DO concentration was increased according to the nitrification response during the experiment. The DO concentration was found to be low to guarantee a steady nitrification activity. In phase IV, increasing the DO concentration in the range of 0.3−0.9 mg/L allowed a better ammonium removal (Fig. 2(a)). Once the ammonium concentration in the influent was increased, a higher DO concentration was required in order to achieve a high nitrification efficiency. However, a DO concentration in the range of 0.8−1.5 mg/L reduced the denitrification efficiency (Fig. 2(b)) but was the maximum limit to guarantee a nitrate concentration in the effluent below the regulation threshold. This agreed with the findings of Li et al. (2021) who found that under a DO concentration condition of 1.2−1.5 mg/L, the denitrification efficiency decreased to 60% with an effluent NO_3^--N concentration of 14.9 mg/L. Moreover, the denitrifying bacteria in phases VI and VII achieved NLRs of 108.4 mg/(L·d) and 139.5 mg/(L·d), respectively. This was similar to 142.2 mg/(L·d) found in Carboni et al. (2022). However, Carboni et al. (2022) treated the nitrogen-contaminated wastewater with only nitrate and with no ammonium. Thus, anoxic conditions were guaranteed throughout the experiment.

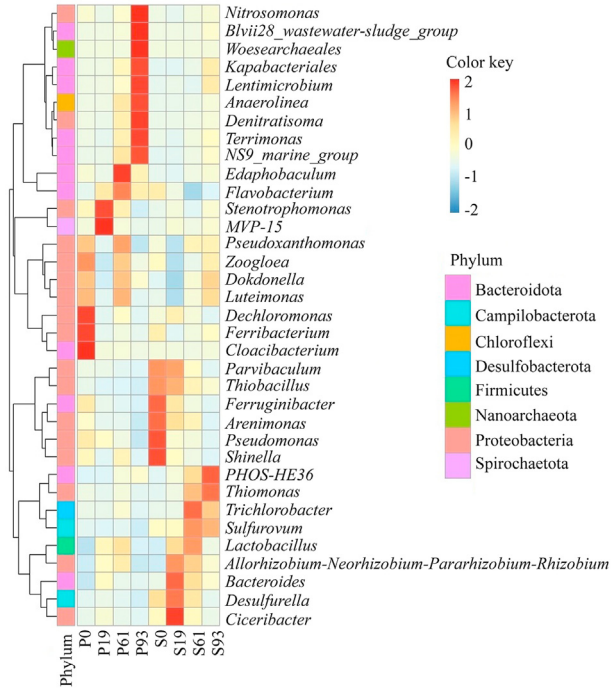

Fig. 7. Cluster heatmap of taxonomic abundance according to top 35 genera of all samples.

4.2. Simultaneous nitrification and autotrophic denitrification with sulfur as electron donor

SNAD in the SR did not exhibit a good performance during all the reactor runs, and very low and unstable nitrification activities were detected (Fig. 2(a)). This could result from the competition for the available oxygen between sulfur oxidizing bacteria in the microbial consortia of the inoculum (e.g., *Thiobacillus* and *Sulfurovum* sp.) (Fig. 7) and ammonium oxidizing bacteria (AOB) (e.g., *Nitrosomonas* with an RA of 0.1%−0.3% during the experiment) (Dytczak et al., 2008). Another possible reason for the inefficient nitrification might be that some sulfur reduction might have occurred with the production of sulfide from elemental sulfur in certain areas of the reactor. No organic carbon was present in the reactor, which could act as an electron donor for the reduction of elemental sulfur. However, Yang et al. (2017) reported that such sulfide production could occur even

only with the contribution of the endogenous carbon of the microorganisms in the system or possible detached biofilm biomass. Even though no sulfide was found in the effluent of the SR FBR according to the spectrophotometric analysis, typical sulfide odor was detectable when solid samples were withdrawn, indicating the possibility of such reductive reactions. A soluble sulfide concentration no greater than 1 mg/L was sufficient to partially or completely inhibit the ammonium oxidizing activity (Beristain-Cardoso et al., 2010; Erguder et al., 2008). These results were in contrast with the findings of Hwang et al. (2005). They investigated simultaneous nitrification−denitrification in a 2.9 L single reactor unit using ciliated columns packed with granular elemental sulfur. The applied synthetic wastewater had a TN concentration of 31.3−52.2 mg/L almost totally in the form of NH_4^+, and the DO concentration varied between 1.0 mg/L and 4.5 mg/L. Moreover, COD at a concentration of 30−66 mg/L was also provided when Hwang et al. (2005) aimed to investigate the possible contribution of sulfur-driven autotrophic denitrification to the conventional heterotrophic denitrification. They achieved an autotrophic TN removal of 200 mg/(L·d) (measured with a control reactor), with no consideration of heterotrophic denitrification. Due to the excessive air bubbles that sloughed the biofilm, the nitrogen removal efficiency decreased when the DO concentration exceeded 4.0 mg/L.

In this study, the three tested DO concentration ranges (0.1−0.3 mg/L, 0.3−0.9 mg/L, and 0.8−1.5 mg/L) in the SR did not limit the denitrification efficiency that was always higher than 90% (Fig. 2(b)). This indicated that a quite robust and specialized microbial community of elemental sulfur oxidizing−nitrate reducing bacteria already existed in the inoculum (see details in Carboni et al. (2022)). This study achieved a maximum NLR of 102.7 mg/(L·d). As reported by Kostrytsia et al. (2018), the high denitrification activity could be due to the application of elemental sulfur in small particles (150 μm in diameter) with a large specific surface area, thereby increasing S^0 solubilization. This assures better contact between sulfur particles and microorganisms. Moreover, the application of an FBR configuration guarantees better dissolution kinetics (Di Capua et al., 2015).

This study found some erratic results. Therefore, a more in-depth investigation of simultaneous nitrification and autotrophic denitrification using elemental sulfur as electron donor is essential. A strategy for future studies could be the treatment of wastewater contaminated only with nitrogen in the form of ammonium as reported by Hwang et al. (2005) in order to force the activity of AOB by starting from a low ammonium concentration and then gradually increasing it. Moreover, the introduced oxygen in this way would be likely to be directly used for nitrification, creating less possible instability for denitrification. The acclimatation of a solely nitrifying community in a reactor for a certain period requires continuous monitoring of the DO concentration in order to keep the community in microaerophilic conditions. This could help to establish a good nitrification performance. The subsequent addition of an enriched denitrifying microbial community could stimulate the simultaneous activity of the two consortia. The fact is that the two microbial communities are both autotrophic. We should not make one prevail over the other because both communities have low growth yields. In contrast, when heterotrophic and autotrophic communities are together in the same environment, heterotrophic species grow faster and often predominate over autotrophic species, making the co-existence of the two types of microorganisms (and consequentially, the two processes) infeasible (Gupta et al., 2021).

4.3. Microbial community

During the complete experiment, one of the dominant families present in both FBRs was Comamonadaceae (Fig. 6(b)). It is a big family that includes various types of microorganisms with several autotrophic denitrifying genera, such as *Acidovorax* sp., *Comamonas* sp., and *Comamonadaceae bacterium* sp. They have been found in elemental sulfur-driven (Kostrytsia et al., 2018), pyrite-driven (Carboni et al., 2021), and thiosulfate-driven (Hao et al., 2017) autotrophic denitrification systems.

The inoculum of the PR had a mixture of other autotrophic denitrifying bacteria (Fig. 7), such as *Cloacibacterium*, *Ferribacterium*, and *Dechloromonas* genera. They have been reported to be able to reduce nitrate (Han et al., 2020; Tan et al., 2021; Zhou et al., 2017). Moreover, *Ferribacterium* sp. has been reported by Tan et al. (2021) to be the dominant genus of a heterotrophic nitrification−aerobic denitrification system that simultaneously removed ammonium and nitrate. At the end of the reactor run (day 93), other autotrophic denitrifiers that could reduce nitrate in aerobic conditions were present in the PR, such as *Terrimonas* sp. and *Denitratisoma* sp. (Liu et al., 2020; Xia et al., 2019). The nitrifying genus *Nitrosomonas* was also detected on day 93 (Fig. 7) in the PR with an RA of only 1%.

In addition to the Comamonadaceae family, the autotrophic denitrifying bacteria *Thiobacillus* and *Sulfurovum* were always present with high RAs during the operation of the SR FBR (Fig. 7). *Thiomonas* and *PHOS-HE36* (belonging to the Ignavibacteriales order) genera became dominant on day 93, which has been reported in previous sulfur-based autotrophic denitrification studies (Han et al., 2020; Carboni et al., 2022). The RA of the *Trichlorobacter* genus (from the Geobacteraceae family) increased to approximately 10% on days 61 and 93, which was reported by Koenig et al. (2005) who reduced elemental sulfur to hydrogen sulfide using organic carbon as the electron donor. This could explain the inhibition of nitrifying bacteria because the endogenous organic carbon might act as an electron donor for sulfur reduction, with produced toxic sulfide in the nitrification pathway.

4.4. Practical applications

The PR FBR was a suitable configuration to simultaneously remove ammonium and nitrate in a single-stage reactor. According to the results of this study, a maximum DO concentration of 1.5 mg/L should be adopted to treat the nitrogen-contaminated wastewater (with an NLR of 145.6 mg/(L·d)) to achieve an effluent nitrate concentration below the regulatory limits. Compared with the conventional separated

autotrophic nitrification−heterotrophic denitrification, the application of such a compact configuration has several advantages. SNAD in microaerobic conditions results in reduced aeration costs, reduced volumes required for wastewater treatment plants due to the occurrence of the two processes in the same reactor, a higher reduction of CO_2 emission than the conventional heterotrophic denitrification, and reduced amounts of produced sludge. Moreover, to treat 1 mg of NH_4^+-N, a conventional nitrification process consumes 7.1 mg of $CaCO_3$ of alkalinity per liter (Iannacone et al., 2019), which has already been endogenously supplied in the pyrite-based SNAD in the proposed configuration due to the production of $Fe(OH)_3$ during the autotrophic denitrification process. All these characteristics of SNAD with pyrite as an electron donor result in decreased investment and operational costs. The low sulfate production in solubilized form and its precipitation as iron sulfate minerals make the process more suitable for wastewater treatment with the aim of water reuse in industrial/agricultural sectors (not only for its discharge in water bodies). This is extremely positive for the whole process due to the following two aspects: (1) the clean water effluent from an FBR does not exhibit high SO_4^{2-} concentrations that could bring secondary problems in drinking water, such as laxative effects (limit of 250 mg/L) (Ashok and Hait, 2015), and (2) solid precipitates can be removed from the reactor and valorized. Iron sulfate is a high-value chemical compound with applications in medicine and wastewater treatment (Ferreira et al., 2021). Moreover, when heat-treated, it produces hematite, a pigment used in the ceramic industry and a catalyst for degradation of colorants and other pollutants in advanced oxidative processes (Ferreira et al., 2021).

Additional studies are required to investigate the response of microorganisms to wastewater polluted with ammonium solely (not with a mixture of ammonium and nitrate) in order to test wastewater with the characteristics of an effluent coming from a previously anaerobic digestion phase. Further studies on pilot/real-scale applications are required to confirm the results of this study.

5. Conclusions

A maximum DO concentration of 1.5 mg/L was beneficial for the simultaneous removal of NH_4^+ and NO_3^- in the FBR with pyrite as an electron donor. The highest nitrogen removal efficiency was achieved to be 139.5 mg/(L·d), and almost no SO_4^{2-} was present in solubilized form in the effluent of the reactor. Instead, SO_4^{2-} was found in the solid compounds precipitated in the reactor in forms of iron sulfates ($FeSO_4$/$Fe_2(SO_4)_3$) and sodium sulfate (Na_2SO_4). However, SNAD with elemental sulfur as an electron donor was not achieved due to the low and unstable ammonium removal in the FBR. On the other hand, this study showed a high nitrate removal efficiency in the S^0-based autotrophic denitrification system, even in the presence of oxygen up to 1.5 mg/L. Thus, a maximum NO_3^--N removal efficiency of 102.7 mg/(L·d) was achieved, which corresponded to a denitrification efficiency of 97.8% during the complete trial experiment. The microbial communities of the two FBRs were both dominated by the Comamonadaceae family. Moreover, in the pyrite-based FBR, the predominant genera at the end of the experiment were *Terrimonas* sp., *Ferruginibacter* sp., and *Denitratimonas* sp., while *Thiobacillus* sp., *Sulfurovum* sp., and *Trichlorobacter* sp. dominated the community in the sulfur FBR. SNAD with pyrite-based FBRs is proved to be a more efficient compact design compared to the conventional configuration (autotrophic nitrification and heterotrophic denitrification) for the treatment of nitrogen-rich wastewater. Before this technique is applied to pilot-scale reactors, further research should be conducted, with major focuses on (1) the quantification of the possibility of incomplete denitrification and the potential NO and N_2O emissions into the atmosphere and (2) the study on the precipitated material in pyrite reactors considering the possibility of recovery of high valuable products.

Declaration of competing interest

The authors declare no conflicts of interest.

Acknowledgements

The authors thank Borja Khatabi Soliman Tamayo, Leah Egan, and Manuel Suarez, at the National University of Ireland Galway, in Ireland, for their help and support during the laboratory work.

References

Ashok, V., Hait, S., 2015. Remediation of nitrate-contaminated water by solid-phase denitrification process−a review. Environ. Sci. Pollut. Control Ser. 22(11), 8075−8093. https://doi.org/10.1007/s11356-015-4334-9.

Beristain-Cardoso, R., Gómez, J., Méndez-Pampín, R., 2010. The behavior of nitrifying sludge in presence of sulfur compounds using a floating biofilm reactor. Bioresour. Technol. 101(22), 8593. https://doi.org/10.1016/j.biortech.2010.06.084, 8098.

Bosch, J., Lee, K.Y., Jordan, G., Kim, K.W., Meckenstock, R.U., 2012. Anaerobic, nitrate-dependent oxidation of pyrite nanoparticles by *Thiobacillus denitrificans*. Environ. Sci. Technol. 46(4), 2095. https://doi.org/10.1021/es2022329, 2101.

Carboni, M.F., Florentino, A.P., Costa, R.B., Zhan, X., Lens, P.N.L., 2021. Enrichment of autotrophic denitrifiers from anaerobic sludge using sulfurous electron donors. Front. Microbiol. 12, 678323. https://doi.org/10.3389/fmicb.2021.678323.

Carboni, M.F., Mills, S., Arriaga, S., Collins, G., Ijaz, U.Z., Lens, P.N.L., 2022. Autotrophic denitrification of high-nitrate wastewater in fluidized bed reactor using pyrite and elemental sulfur as electron donors. Environ. Technol. Innovat. 28, 102878. https://doi.org/10.1016/j.eti.2022.102878.

Cardoso, R.B., Sierra-Alvarez, R., Rowlette, P., Flores, E.R., Gómez, J., Field, J.A., 2006. Sulfide oxidation under chemolithoautotrophic denitrifying conditions. Biotechnol. Bioeng. 95(6), 1148−1157. https://doi.org/10.1002/bit.21084.

Chen, X., Guo, J., Xie, G., Liu, Y., Yuan, Z., Ni, B., 2015. A new approach to simultaneous ammonium and dissolved methane removal from anaerobic digestion liquor: A model-based investigation of feasibility. Water Res. 85, 295−303. https://doi.org/10.1016/j.watres.2015.08.046.

Chung, J., Amin, K., Kim, S., Yoon, S., Kwon, K., Bae, K., 2014. Autotrophic denitrification of nitrate and nitrite using thiosulfate as an electron donor. Water Res. 58, 169−178. https://doi.org/10.1016/j.watres.2014.03.071.

Di Capua, F., Papirio, S., Lens, P.N.L., Esposito, G., 2015. Chemolithotrophic denitrification in biofilm reactors. Chem. Eng. J. 280, 643−657. https://doi.org/10.1016/j.cej.2015.05.131.

Di Capua, F., Pirozzi, F., Lens, P.N.L., Esposito, G., 2019. Electron donors for autotrophic denitrification. Chem. Eng. J. 362, 922−937. https://doi.org/10.1016/j.cej.2019.01.069.

Di Capua, F., Mascolo, M.C., Pirozzi, F., Esposito, G., 2020. Simultaneous denitrification, phosphorus recovery and low sulfate production in a recirculated pyrite-packed biofilter (RPPB). Chemosphere 255, 126977. https://doi.org/10.1016/j.chemosphere.2020.126977.

Dolejs, P., Paclík, L., Maca, J., Pokorna, D., Zabranska, J., Bartacek, J., 2015. Effect of S/N ratio on sulfide removal by autotrophic denitrification. Appl. Microbiol. Biotechnol. 99(5), 2383−2392. https://doi.org/10.1007/s00253-014-6140-6.

Drewnowski, J., Shourjeh, M.S., Kowal, P., Cel, W., 2021. Modelling AOB-NOB competition in shortcut nitrification compared with conventional nitrification−denitrification process. J. Phys. Conf. 1736(1), 012046. https://doi.org/10.1088/1742-6596/1736/1/012046.

Dytczak, M.A., Londry, K.L., Oleszkiewicz, J.A., 2008. Activated sludge operational regime has significant impact on the type of nitrifying community and its nitrification rates. Water Res. 42(8−9), 2320−2328. https://doi.org/10.1016/j.watres.2007.12.018.

Erguder, T.H., Boon, N., Vlaeminck, S.E., Verstraete, W., 2008. Partial nitrification achieved by pulse sulfide doses in a sequential batch reactor. Environ. Sci. Technol. 42(23), 8715−8720. https://doi.org/10.1021/es801391u.

Evangelou, V.P., Zhang, Y.L., 1995. A review: Pyrite oxidation mechanisms and acid mine drainage prevention. Crit. Rev. Environ. Sci. Technol. 25(252), 37−41. https://doi.org/10.1080/10643389509388477.

Ferreira, L.P., Müller, T.G., Cargnin, M., De Oliveira, C.M., Peterson, M., 2021. Valorization of waste from coal mining pyrite beneficiation. J. Environ. Chem. Eng. 9(4), 105759. https://doi.org/10.1016/j.jece.2021.105759.

Florentino, A.P., Costa, R.B., Hu, Y., Flaherty, V.O., Lens, P.N.L., 2020. Long chain fatty acid degradation coupled to biological sulfidogenesis: A prospect for enhanced metal recovery. Front. Bioeng. Biotechnol. 8, 550253. https://doi.org/10.3389/fbioe.2020.550253.

Guerrero, R.B.S., Zaiat, M., 2018. Wastewater post-treatment for simultaneous ammonium removal and elemental sulfur recovery using a novel horizontal mixed aerobic-anoxic fixed-bed reactor configuration. J. Environ. Manag. 215, 358−365. https://doi.org/10.1016/j.jenvman.2018.03.074.

Gupta, R.K., Poddar, B.J., Nakhate, S.P., Chavan, A.R., Singh, A.K., Purohit, H.J., Khardenavi, A.A., 2021. Role of heterotrophic nitrifiers and aerobic denitrifiers in simultaneous nitrification and denitrification process: A nonconventional nitrogen removal pathway in wastewater treatment. Lett. Appl. Microbiol. 74(2), 159−184. https://doi.org/10.1111/lam.13553.

Hakanen, J., Miettinen, K., Sahlstedt, K., 2011. Wastewater treatment: New insight provided by interactive multiobjective optimization. Decis. Support Syst. 51(2), 328−337. https://doi.org/10.1016/j.dss.2010.11.026.

Han, F., Zhang, M., Shang, H., Liu, Z., Zhou, W., 2020. Microbial community succession, species interactions and metabolic pathways of sulfur-based autotrophic denitrification system in organic limited nitrate wastewater. Bioresour. Technol. 315, 123826. https://doi.org/10.1016/j.biortech.2020.123826.

Hao, R., Meng, G., Li, J., 2017. Impact of operating condition on the denitrifying bacterial community structure in a 3DBER-SAD reactor. J. Ind. Microbiol. Biotechnol. 44(1), 9−21. https://doi.org/10.1007/s10295-016-1853-4.

Hoffmann, H., Da Costa, T.B., Wolff, D.B., Platzer, C., Da Costa, R.H.R., 2007. The potential of denitrification for the stabilization of activated sludge processes affected by low alkalinity problems. Braz. Arch. Biol. Technol. 50(2), 329−337. https://doi.org/10.1590/S1516-89132007000200018.

Hwang, Y.W., Kim, C.G., Choo, I.J., 2005. Simultaneous nitrification/denitrification in a single reactor using ciliated columns packed with granular sulfur. Water Qual. Res. J. Can. 40(1), 91−96. https://doi.org/10.2166/wqrj.2005.008.

Iannacone, F., Di Capua, F., Granata, F., Gargano, R., Pirozzi, F., Esposito, G., 2019. Effect of carbon-to-nitrogen ratio on simultaneous nitrification denitrification and phosphorus removal in a microaerobic moving bed biofilm reactor. J. Environ. Manag. 250, 109518. https://doi.org/10.1016/j.jenvman.2019.109518.

Jiang, L., Chen, X., Qin, M., Cheng, S., Wang, Y., Zhou, W., 2019. On-board saline black water treatment by bioaugmentation original marine bacteria with *Pseudoalteromonas* sp. SCSE709-6 and the associated microbial community. Bioresour. Technol. 273, 496−505. https://doi.org/10.1016/j.biortech.2018.11.043.

Jørgensen, C.J., Jacobsen, O.S., Elberling, B., Aamand, J., 2009. Microbial oxidation of pyrite coupled to nitrate reduction in anoxic groundwater sediment. Environ. Sci. Technol. 43(13), 4851−4857. https://doi.org/10.1021/es803417s.

Kadam, S.S., Mesbah, A., Van Der Windt, E., Kramer, H.J.M., 2010. Rapid online calibration for ATR-FTIR spectroscopy during batch crystallization of ammonium sulphate in a semi-industrial scale crystallizer. Chem. Eng. Res. Des. 89(7), 995−1005. https://doi.org/10.1016/j.cherd.2010.11.013.

Kiefer, J., Srärk, A., Kiefer, A.L., Glade, H., 2018. Infrared spectroscopic analysis of the inorganic deposits from water in domestic and technical heat exchangers. Energies 11(4), 798. https://doi.org/10.3390/en11040798.

Koenig, A., Zhang, T., Liu, L., Fang, H.H.P., 2005. Microbial community and biochemistry process in autosulfurotrophic denitrifying biofilm. Chemosphere 58, 1041−1047. https://doi.org/10.1016/j.chemosphere.2004.09.040.

Kostrytsia, A., Papirio, S., Frunzo, L., Mattei, M.R., Porca, E., Collins, G., Lens, P.N.L., Esposito, G., 2018. Elemental sulfur-based autotrophic denitrification and denitritation: Microbially catalyzed sulfur hydrolysis and nitrogen conversions. J. Environ. Manag. 211, 313−322. https://doi.org/10.1016/j.jenvman.2018.01.064.

Lehner, S., Savage, K., Ciobanu, M., Cliffel, D.E., 2007. The effect of As, Co, and Ni impurities on pyrite oxidation kinetics: An electrochemical study of synthetic pyrite. Geochem. Cosmochim. Acta 71(10), 2491−2509. https://doi.org/10.1016/j.gca.2007.03.005.

Li, H., Li, Y., Guo, J., Song, Y., Hou, Y., Lu, C., Han, Y., Shen, X., Liu, B., 2021. Effect of calcinated pyrite on simultaneous ammonia, nitrate and phosphorus removal in the BAF system and the Fe^{2+} regulatory mechanisms: Electron transfer and biofilm properties. Environ. Res. 194(3), 110708. https://doi.org/10.1016/j.envres.2021.110708.

Li, Y., Guo, J., Li, H., Song, Y., Chen, Z., Lu, C., Han, Y., Hou, Y., 2020. Effect of dissolved oxygen on simultaneous removal of ammonia, nitrate and phosphorus via biological aerated filter with sulfur and pyrite as composite fillers. Bioresour. Technol. 296, 122340. https://doi.org/10.1016/j.biortech.2019.122340.

Liu, T., He, X., Jia, G., Xu, J., Quan, X., You, S., 2020. Simultaneous nitrification and denitrification process using novel surface-modified suspended carriers for the treatment of real domestic wastewater. Chemosphere 247, 125831. https://doi.org/10.1016/j.chemosphere.2020.125831.

Majzlan, J., Alpers, C.N., Bender, C., Mccleskey, R.B., Myneni, S.C.B., Neil, J.M., 2011. Vibrational, X-ray absorption, and Mössbauer spectra of sulfate minerals from the weathered massive sulfide deposit at Iron Mountain, California. Chem. Geol. 284(3−4), 296−305. https://doi.org/10.1016/j.chemgeo.2011.03.008.

Mora, M., López, L.R., Lafuente, J., Pérez, J., Kleerebezem, R., van Loosdrecht, M.C.M., Gamisans, X., Gabriel, D., 2016. Respirometric characterization of aerobic sulfide, thiosulfate and elemental sulfur oxidation by S-oxidizing biomass. Water Res. 89, 282−292. https://doi.org/10.1016/j.watres.2015.11.061.

Park, J., Jin, H., Lim, B., Park, K., Lee, K., 2010. Bioresource technology ammonia removal from anaerobic digestion effluent of livestock waste using green alga *Scenedesmus* sp. Bioresour. Technol. 101(22), 8649−8657. https://doi.org/10.1016/j.biortech.2010.06.142.

Pochana, K., Keller, J., 1999. Study of factors affecting simultaneous nitrification and denitrification (SND). Water Sci. Technol. 39(6), 61−68. https://doi.org/10.1016/S0273-1223(99)00123-7.

Pu, J., Feng, C., Liu, Y., Li, R., Kong, Z., Chen, N., Tong, S., Hao, C., Liu, Y., 2015. Pyrite-based autotrophic denitrification for remediation of nitrate contaminated groundwater. Bioresour. Technol. 173, 117−123. https://doi.org/10.1016/j.biortech.2014.09.092.

Shao, M., Zhang, T., Fang, H.H.P., 2010. Sulfur-driven autotrophic denitrification: Diversity, biochemistry, and engineering applications. Appl. Microbiol. Biotechnol. 88(5), 1027−1042. https://doi.org/10.1007/s00253-010-2847-1.

Stams, A.J.M., Van Dijk, J.B., Dijkema, C., Plugge, C.M., 1993. Growth of syntrophic propionate-oxidizing bacteria with fumarate in the absence of methanogenic bacteria. Appl. Environ. Microbiol. 59(4), 1114−1119. https://doi.org/10.1128/aem.59.4.1114-1119.1993.

Tan, X., Yang, Y., Liu, Y., Li, X., Zhu, W., 2021. Quantitative ecology associations between heterotrophic nitrification-aerobic denitrification, nitrogen-metabolism genes, and key bacteria in a tidal flow constructed wetland. Bioresour. Technol. 377, 125549. https://doi.org/10.1016/j.biortech.2021.125449.

Xia, Z., Wang, Q., Shea, Z., Gao, M., Zhao, Y., Guo, L., Jin, C., 2019. Nitrogen removal pathway and dynamics of microbial community with the increase of salinity in simultaneous nitrification and denitrification process. Sci. Total Environ. 697, 134047. https://doi.org/10.1016/j.scitotenv.2019.134047.

Yang, Y., Chen, T., Morrison, L., Gerrity, S., Collins, G., Porca, E., Li, R., Zhan, X., 2017. Nanostructured pyrrhotite supports autotrophic denitrification for simultaneous nitrogen and phosphorus removal from secondary effluents. Chem. Eng. J. 328, 511−518. https://doi.org/10.1016/j.cej.2017.07.061.

Zhou, W., Li, Y., Liu, X., He, S., Huang, J.C., 2017. Comparison of microbial communities in different sulfur-based autotrophic denitrification reactors. Appl. Microbiol. Biotechnol. 101, 447−453. https://doi.org/10.1007/s00253-016-7912-y.